Support vector machine-based assessment of the T-wave morphology improves long QT syndrome diagnosis

Please check the document version of this publication:

• A submitted manuscript is the version of the article upon submission and before peer-review. There can be important differences between the submitted version and the official published version of record. People interested in the research are advised to contact the author for the final version of the publication, or visit the DOI to the publisher's website.
• The final author version and the galley proof are versions of the publication after peer review.
• The final published version features the final layout of the paper including the volume, issue and page numbers.

Link to publication

ORIGINAL RESEARCH

Support vector machine-based assessment of the T-wave morphology improves long QT syndrome diagnosis

Ben J.M. Hermans[1,2,3†], Job Stoks[1,2,4†], Frank C. Bennis[1,5], Arja S. Vink[6], Ainara Garde[7], Arthur A.M. Wilde[6], Laurent Pison[3], Pieter G. Postema[6], and Tammo Delhaas[1,2]*

[1]Department of Biomedical Engineering, Maastricht University, PO Box 616, 6200 MD Maastricht, The Netherlands; [2]Cardiovascular Research Institute Maastricht (CARIM), Maastricht University, PO Box 616, 6200 MD Maastricht, The Netherlands; [3]Department of Cardiology, Maastricht University Medical Centre, PO Box 5800, 6202 AZ Maastricht, The Netherlands; [4]MIRA Institute for Biomedical Technology and Technical Medicine, University of Twente, PO Box 217, 7500 AE Enschede, The Netherlands; [5]MHeNS School for Mental Health and Neuroscience, Maastricht University, PO Box 616, 6200 MD Maastricht, The Netherlands; [6]Heart Centre, Department of Clinical and Experimental Cardiology, Academic Medical Center, PO Box 22660, 1100 DD Amsterdam, the Netherlands; and [7]Department of Biomedical Signals and Systems, Faculty EEMCS, University of Twente, PO Box 217, 7500 AE Enschede, The Netherlands

Aims	Diagnosing long QT syndrome (LQTS) is challenging due to a considerable overlap of the QTc-interval between LQTS patients and healthy controls. The aim of this study was to investigate the added value of T-wave morphology markers obtained from 12-lead electrocardiograms (ECGs) in diagnosing LQTS in a large cohort of gene-positive LQTS patients and gene-negative family members using a support vector machine.
Methods and results	A retrospective study was performed including 688 digital 12-lead ECGs recorded from genotype-positive LQTS patients and genotype-negative relatives at their first visit. Two models were trained and tested equally: a baseline model with age, gender, RR-interval, QT-interval, and QTc-intervals as inputs and an extended model including morphology features as well. The best performing baseline model showed an area under the receiver-operating characteristic curve (AUC) of 0.821, whereas the extended model showed an AUC of 0.901. Sensitivity and specificity at the maximal Youden's indexes changed from 0.694 and 0.829 with the baseline model to 0.820 and 0.861 with the extended model. Compared with clinically used QTc-interval cut-off values (>480 ms), the extended model showed a major drop in false negative classifications of LQTS patients.
Conclusion	The support vector machine-based extended model with T-wave morphology markers resulted in a major rise in sensitivity and specificity at the maximal Youden's index. From this, it can be concluded that T-wave morphology assessment has an added value in the diagnosis of LQTS.
Keywords	QT-interval • T-wave • Morphology • Long QT syndrome • Machine learning

Introduction

Long QT syndrome (LQTS) is an inheritable disease entity associated with malignant arrhythmias at young age. The diagnosis of congenital LQTS, once based on a scoring system of clinical and electrocardiographic parameters, is nowadays aided by genetic testing. Despite the fact that genetic testing is currently relatively easy to perform at relatively low costs, it remains of utmost importance to preserve genetic testing to persons suspected for LQTS, since distinguishing pathogenic variants from innocuous rare variants can be very complex.[1] To identify persons suspected for LQTS, gender-based cut-off values for a prolonged QT-interval corrected for heart rate (QTc) are used.

> **What's new?**
> - The added value of T-wave morphology markers on standard 10-s resting electrocardiograms to diagnose Long QT syndrome (LQTS) was investigated.
> - The cohort consisted of only genotype-positive LQTS patients and their genotype-negative family members.
> - T-wave morphology was assessed automatically.
> - A support vector-machine was used to combine various T-wave morphology markers to improve LQTS diagnosis.

However, it is known that there is a considerable overlap in QTc-intervals between LQTS patients and healthy controls,[2] which hampers the accuracy of diagnosing LQTS based on the QTc-interval. Therefore, attempts have been made to take advantage of the fact that LQTS patients often display abnormal responses to heart rate changes. This led to diagnostic interventions in which the QT-interval adaptation to heart rate changes is studied in for example the exercise recovery phase,[3] after epinephrine provocation,[4] and the brisk-standing-test.[5] Although these interventions are known to improve LQTS diagnosis, a clinician should have an LQTS suspicion before such a test will be performed. Long QT syndrome patients with a normal QTc-interval on the resting electrocardiograms (ECG) are likely to never be tested with such an interventional diagnostic test when they are not overt symptomatic or become part of a family evaluation for LQTS and may therefore remain undiagnosed. Still, they may have exaggerated risks for malignant arrhythmias under particular conditions such as the use of certain drugs and they may have children who can become severely symptomatic when undiagnosed.[6]

Apart from a prolongation of the QTc-interval, variations in the morphological configuration of the T-wave are seen in LQTS patients, especially in relation to the LQTS type.[7,8] Previous studies have indicated that using T-wave morphologies during interventions as an additional marker to diagnose LQTS improves the diagnosis.[9,10] These studies however not only require an intervention but their manual assessment of T-wave morphologies makes the results clinician dependent.

The added value of T-wave morphology markers in standard 10-s 12-lead ECGs to identify possibly LQTS genotype-positive patients of the three most common mutated genes has not yet been investigated. In this study, we use a machine-learning approach to investigate the added value of T-wave morphology markers obtained from baseline 10-s 12-lead body surface ECGs to diagnose LQTS in a large cohort of gene-positive LQTS patients and their gene-negative family members.

Methods

Study population

A retrospective cohort study consisting of LQTS patients and their family was performed. Long QT syndrome patients with LQTS Type 1 (LQT1), Type 2 (LQT2), and Type 3 (LQT3) were confirmed by pathogenic variants in *KCNQ1*, *KCNH2*, or *SCN5A*, respectively. All genotype-negative family members were used as healthy controls. All individuals were seen in the Academic Medical Centre in Amsterdam, The Netherlands,

between January 1996 and December 2016. Inclusion criteria for this study were an age ≥16 years, known genetic testing results and digitally available ECG at first presentation. Exclusion criteria were the presence of any comorbidity that might affect ventricular re- and/or depolarization. The study was approved by the Academic Medical Center Review Board and informed consent of the individuals was waived as this study used retrospective data from regular care.

Electrocardiograms

Digital standard 10-s 12-leads body surface ECGs performed in the initial evaluation of individuals in the work-up during (family) screening for LQTS were collected. Electrocardiograms were excluded when the ECG contained too much noise and when all T-waves in all ECG leads were too flat (<40 μV) to reliably assess the QT-interval and T-wave morphology automatically. To avoid subjective evaluation of the T-wave morphology, all ECG landmarks and T-wave morphology features were calculated automatically using custom-made software in MATLAB (2017a, Mathworks, Natick, MA, USA).

Data acquisition and pre-processing

Electrocardiograms were stored in the MUSE Cardiology Information system (GE Healthcare, Little Chalfont, UK) and recorded with a 250 or 500 Hz sample frequency. All further processing and analyses in this study were done using custom-made software in MATLAB. Electrocardiograms were first filtered using a 2nd order bidirectional Butterworth band pass filter (0.5–125 Hz) and a 2nd order infinite impulse response notch filter (50 Hz). For all individual ECG leads, the residuals of a median filter with a 600 ms window were regarded as baseline deviations and were therefore subtracted from the individual leads to correct for baseline wander. After filtering, a one-dimensional Fourier up-sampling method was used to up-sample all ECG data to 1 kHz to assure sampling frequency independency of our analysis.

Average complex construction

To obtain the best signal-to-noise ratio, analysis was done on average complexes as constructed for all individual ECG leads. To construct these average complexes, first all R-peaks were detected in the ECG lead with the highest R-peak amplitude using a modified Pan-Tompkins algorithm.[11] From these R-peaks, a trimmed mean RR-interval was calculated after omitting 10% of the outermost RR-intervals. The individual complexes were selected from the R-peak location minus 25% of the trimmed mean RR-interval to the R-peak plus 70% of the trimmed mean RR-interval. All complexes were aligned on the R-peak and an average complex was calculated. Thereafter, to guarantee averaging of only reliable complexes, individual complexes with a correlation coefficient below 0.9 when correlated with the average complex as well as complexes with an RR-interval deviating more than 20% from the mean RR were excluded. If less than 60% of all complexes in the whole ECG were preserved after these exclusions, the entire ECG was excluded for further analysis.

Furthermore, if less than 60% of all complexes in an individual lead were preserved, the entire lead was not taken into account since no reliable average complex could be constructed for this lead. Finally, if a complex was excluded in more than three leads, the complex was excluded for all leads to guarantee exclusion of e.g. ventricular extra systoles into the average complex. A new and final average complex for all remaining ECGs and leads was constructed from all remaining complexes. These final average complexes were used for further analysis.

Landmark detection

To detect a global R-peak and QRS-onset, a root mean square ECG (ECG$_{RMS}$) was constructed from the precordial leads and the

Table 1 **T-wave morphology features summary**

Features	Short descriptions	Calculated for	References
Area	Integral over time of T-wave amplitudes (can be negative and positive)	VR, VL, VF, V1–V6	–
Absolute area	Integral over time of absolute T-wave amplitudes	VR, VL, VF, V1–V6	–
Length	Interval between T_{start} and T_{end}	PCA$_1$	–
Biphasicness	$1 - \frac{|Area|}{Absolute\ area}$ (1 = biphasic, 0 = not biphasic)	VR, VL, VF, V1–V6	–
Amplitude	Height of the highest absolute value of the T-wave	VR, VL, VF, V1–V6	–
Time to onset	Interval between R and T_{start}	ECG$_{RMS}$ and PCA$_1$	–
Skewness	T-waves were treated as probability distribution curves and normalized	VR, VL, VF, V1–V6	–
Kurtosis	between 0 and 1 before calculating the skewness and kurtosis	VR, VL, VF, V1–V6	–
Notch score	According to Andersen *et al.* but applied on all unipolar ECG leads	VR, VL, VF, V1–V6	[20]
Asymmetry score	instead of only on PCA$_1$	VR, VL, VF, V1–V6	[20]
QRS amplitude	Height of the highest absolute value of the QRS-complex	VR, VL, VF, V1–V6	–
TH$_{V1–V3}$, TH$_{V4–V6}$ RH$_{V1–V3}$, RH$_{V4–V6}$	T-wave and R-peak heterogeneity = max $\left(\sqrt{var(X)}\right)$ in which X is an n-by-3 matrix consisting of three ECG leads of length n.	V1–V3 V4–V6	[22]
SP QRS-T angle	Spatial peak QRS-T angle is the smallest angle between the vector at maximal T-wave magnitude and the vector at maximal QRS complex magnitude in the VCG	VCG	[23]
SM QRS-T angle	Spatial mean QRS-T angle is the smallest angle between the mean vector of the T-wave and the mean vector of the QRS-complex in the VCG	VCG	[23]
T_{peak}-T_{end} interval	Interval between T_{peak} and T_{end}	PCA$_1$	[24]

ECG$_{RMS}$, root mean square of the unipolar ECG leads; PCA$_1$, the first component of principal component analysis; RH, R-peak heterogeneity; SM, spatial mean; SP, spatial peak; TH, T-wave heterogeneity; VCG, vectorcardiogram.

reconstructed unipolar leads VR, VL, VF as described previously by our research group.[12]

The first component of principal component analysis (PCA$_1$) using singular value decomposition on the unipolar ECG leads (VR, VL, VF, and V1–V6) from R-peak + 95 ms to R-peak + 0.7 × RR was used for global T-wave landmarks. The peak of the T-wave (T_{peak}) was detected as the most prominent peak of PCA$_1$. The start and end of the T-wave (T_{start} and T_{end}) were detected by means of an automated tangent method as we described earlier.[12] T_{start} and T_{end} were manually checked by one observer (T.D.) since multiple T-wave morphology features rely on a proper determination of T_{start} and T_{end}.

T-wave morphology features

All T-wave morphology features, apart from the T-wave heterogeneities, were computed within the window T_{start} and T_{end} for all unipolar ECG leads. Most of the features were calculated for all ECG leads individually. For some features, the ECG$_{RMS}$, PCA$_1$ or a vectorcardiogram (reconstructed using the Kors matrix[13]) were used. All computed features are listed in *Table 1*.

Support vector machine
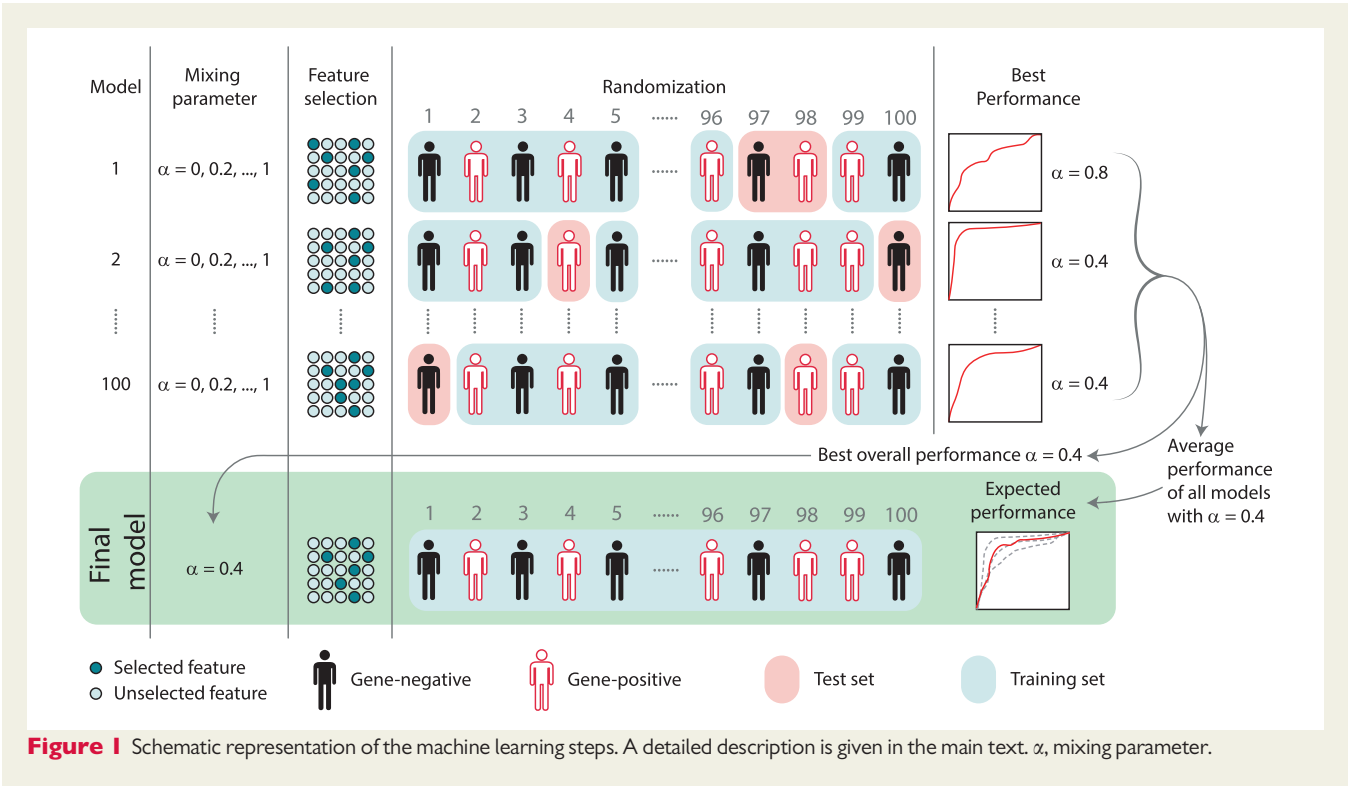
Model inputs

Subjects were classified as gene-positive or gene-negative by a machine learning classification model based on multiple inputs. Missing feature values were replaced by random values within mean ± standard deviation for the corresponding feature. Two models were created: a baseline model with age, gender, RR-interval, QT-interval, and QTc-intervals (QT corrected for heart rate by the correction formulas of Bazett, Fridericia, Framingham and Hodges[14]) as inputs and an extended model with all morphology features as additional model inputs. The performance of the

baseline model was used to determine the optimal classification using commonly used clinical parameters. The difference between the baseline model and the extended model demonstrates the added diagnostic value of T-wave morphology features.

Model training and testing

The model and training used in this study are summarized in *Figure 1*. Both the baseline and the extended model were trained and tested on the ECGs of the entire cohort using cross-validation. Therefore, the performance of these models cannot be assessed directly. Hence, to investigate the performances of the baseline and extended models, 100 similar models were trained and tested on different randomized training and testing sets. This was done for both the baseline and extended model. Training sets consisted of a randomly chosen subset of ECGs containing 90% of all individuals, whereas testing sets consisted of the ECGs of the remaining 10% of all individuals. The mean performance of these 100 models is the expected performance of the final model.[15]

For each of these 100 models, features with the highest discriminative performance were selected by means of elastic net regularization, combined with maximum likelihood estimation in a logistic regression model. For a detailed description of elastic net regularization, we refer to Zou and Hastie.[16] In short, it combines two feature selection methods (lasso and ridge regression). The mixing parameter (α) controls the ratio of both feature selection methods to obtain an optimal combination. The tuning parameter (λ) controls the strength of this optimal combination. For each of the 100 models, during feature selection, the value of α was varied from 0 to 1, with steps of 0.2. For each value of α, 100 values of λ ranging from λ_{max} (at which all features were excluded) to $10^{-4} \cdot \lambda_{max}$ were tested.[17] For each λ, the cross-validated error resulting from 10-fold cross-validation on the current training set was noted. Subsequently,

Figure I Schematic representation of the machine learning steps. A detailed description is given in the main text. α, mixing parameter.

for each α, selected features resulting from the cross-validation were noted at λ_{min} (at the minimal cross-validated error) and λ_{1SE} ($\lambda_{min} + 1$ standard error).

For each of the 100 models, the area under the receiver-operating characteristic curve (AUC) was calculated with each α at λ_{min} and λ_{1SE}. The combination of α and λ with the highest mean AUC over all 100 models was selected as the optimal combination. This α and λ were used in the final model.

Statistical analysis

Values are expressed as mean ± standard deviation. The differences between LQTS patients and genotype-negative family members were analysed by independent samples *T*-test for parametric data, and χ^2 for non-parametric data. A *P*-value <0.05 was considered statistically significant. Receiver-operating characteristic (ROC) analysis was used to determine the performance of the models. Optimal performance was the point with the maximal Youden's index (YI_{max} = sensitivity + specificity − 1). The area AUC, YI_{max}, the sensitivity, and specificity were used to quantify the ability of the different models to diagnose LQTS.

Results

Study population

Of all 1087 individuals with digitally available ECGs in their work-up during (family) screening for LQTS, 284 were <16 years of age and for 48 individuals genetic testing results were unknown. From the remaining 755 individuals eligible for the study, 45 (6.0%) were excluded based on the presence of comorbidities that might potentially affect ventricular re- and/or depolarization (varying from e.g. bundle branch blocks, hypokalaemia, thalassaemia, angina pectoris, an

Table 2   Study population characteristics

|	Number	Gender (male/female)	Age (years)
Control	348	163/185	45 ± 15
LQTS	340	143/197	41 ± 15
LQT1	129	52/77	42 ± 15
LQT2	160	72/88	42 ± 15
LQT3	51	19/32	40 ± 15

Age is given as mean ± standard deviation. All others are presented as counts. LQTS, long QT syndrome; LQT1, LQT2, and LQT3, long QT syndrome Type 1, 2, and 3.

overlap syndrome with Brugada syndrome, to severe post-anoxic encephalopathy). In 11 (1.5%) individuals the ECG registration contained too much noise and in 6 (0.8%) individuals T-waves were too flat (<40 μV) to reliably calculate T_{start} and T_{end}. In 5 (0.7%) individuals a correct ECG export failed. The remaining 688 (91.1%) individuals were included in the analyses. The baseline characteristics of the LQTS patients and the genotype-negative family members are shown in *Table 2*. LQTS patients were statistically significant younger compared with controls (41 ± 15 vs. 45 ± 15 years, *P* < 0.001).

Baseline model

The best performing support vector machine-based baseline model was reached with an α of 1 and an elastic net tuning parameter of λ_{min}. The selected features for the baseline model were: age,
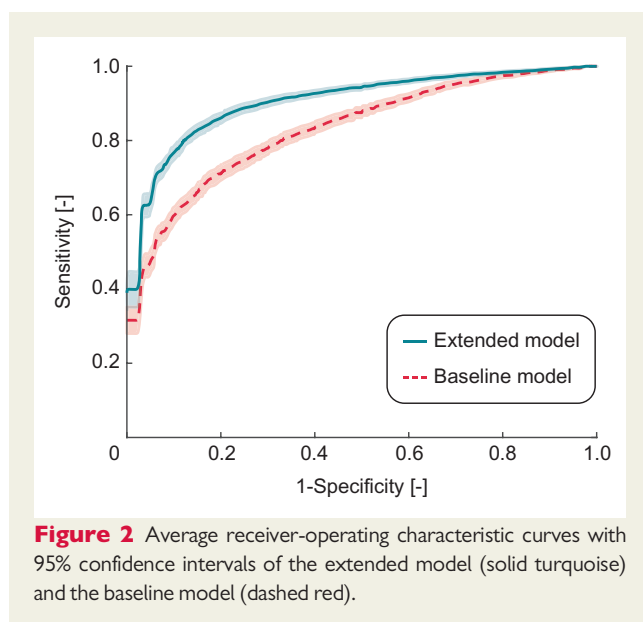
Figure 2 Average receiver-operating characteristic curves with 95% confidence intervals of the extended model (solid turquoise) and the baseline model (dashed red).

Table 3 Selected features

Features	β
Age	-0.010
QT	0.002
QTc Bazett	0.0048
QTc Fridericia	0.0044
QTc Framingham	0.0043
QTc Hodges	0.0048
Area in VL, V2, V3	3.57×10^{-6}, 1.69×10^{-7}, and 1.96×10^{-6}
Absolute area in VL, V1, V2, V3	2.28×10^{-6}, 1.35×10^{-5}, 1.45×10^{-6}, and 4.13×10^{-6}
Biphasicness in VR, V1, V2, V6	-0.51, -0.09, -0.08, and -0.35
Amplitude in VR, VF, V6	5.49×10^{-4}, -1.54×10^{-5}, and -1.35×10^{-4}
Length	0.011
Time to onset	0.007
Skewness in VR, VL, VF, V4, V5, V6	-0.69; -0.24; -0.47; -0.07; -0.40; -0.21
Kurtosis in VL and V3	0.43; 0.30
Asymmetry in VR, VL, VF, V2, V3	1; 0.09; 0.07; 0.03; 0.21
T_{peak} to T_{end} interval	2
QRS amplitude VL, VF, V1	-1.40×10^{-4}, -2.99×10^{-4}, 6.19×10^{-5}
SP QRS-T angle	0.0018
RH_{V4-V6}	-3.00×10^{-4}
TH_{V4-V6}	0.0012

Note that all features are unitless because all features are normalized by subtracting the mean and dividing the result by the standard deviation (with mean and standard deviation determined from the training set).
RH, R-peak heterogeneity; SP, spatial peak; TH, T-wave heterogeneity.

QT-interval, and QTc-Hodges. The ROC of the best performing baseline model is shown in *Figure 2*. ROC analysis resulted in an AUC of 0.821 and a YI_{max} of 0.523 with a corresponding sensitivity and specificity of 0.694 and 0.829, respectively.

Extended model

The best performing support vector machine-based extended model with additional morphology inputs was reached with an α of 0.2 and an elastic net tuning parameter of λ_{1SE}. ROC curves, shown in *Figure 2*, resulted in an AUC of 0.901 (95% CI 0.893–90.87), a YI_{max} of 0.681 and a sensitivity and specificity of 0.820 and 0.861, respectively. All selected features along with their coefficients are listed in *Table 3*. Compared with the baseline model, AUC, sensitivity and specificity increased with 0.080, 0.126, and 0.032, respectively.

Clinical QTc-interval cut-off value

Figure 3 shows the amount of correctly and incorrectly classified cases and controls based on the clinically used QTc-Bazett thresholds (>480 ms[18]) as well as the classification results based on the extended model. As shown in *Figure 3*, the extended model resulted in a major drop of incorrectly classified LQTS patients. It can also be seen that some controls with a QTc-interval >480 ms are correctly classified as control by the extended model. This all comes at the cost of some controls (with QTc-interval <480 ms) being incorrectly classified as LQTS patients.

Discussion

In this study, we compared a baseline model using age, gender, QT- and QTc-interval as inputs with a model extended with T-wave morphology inputs to investigate the added value of T-wave morphology markers in the automated diagnosis of LQTS. Comparison of the ROC analyses of both models showed that the model extended with T-wave morphology markers resulted in a better performance. Since

both models were trained and tested similarly, this improved performance can be attributed to the addition of the T-wave morphology markers. In other words, it can be concluded that T-wave morphology markers have an added value to age, gender, QT- and QTc-interval in automatically distinguishing LQTS patients from genotype-negative family members.

The sensitivity and specificity of respectively 0.820 and 0.861 from our extended model might seem modest to previous studies, which have suggested higher performances when using T-wave markers for the diagnosis of LQTS.[9,19–21] However, our study population consisted of LQTS patients and gene-negative family members, whereas other studies used healthy individuals as controls.[9,19–21] In our study, QTc-intervals of the control group showed considerable more overlap with QTc-intervals of LQTS patients than in the above-mentioned studies. Therefore, distinguishing gene-positive LQTS from gene-negative family members is more challenging than distinguishing LQTS patients from healthy controls. This might explain the higher performance of other studies on the added value of T-wave morphology markers to identify LQTS patients. Beside the use of different control groups, the ECG recordings also differed between our study and the studies by Immanuel *et al.*[19] and Chorin *et al.*[9] who
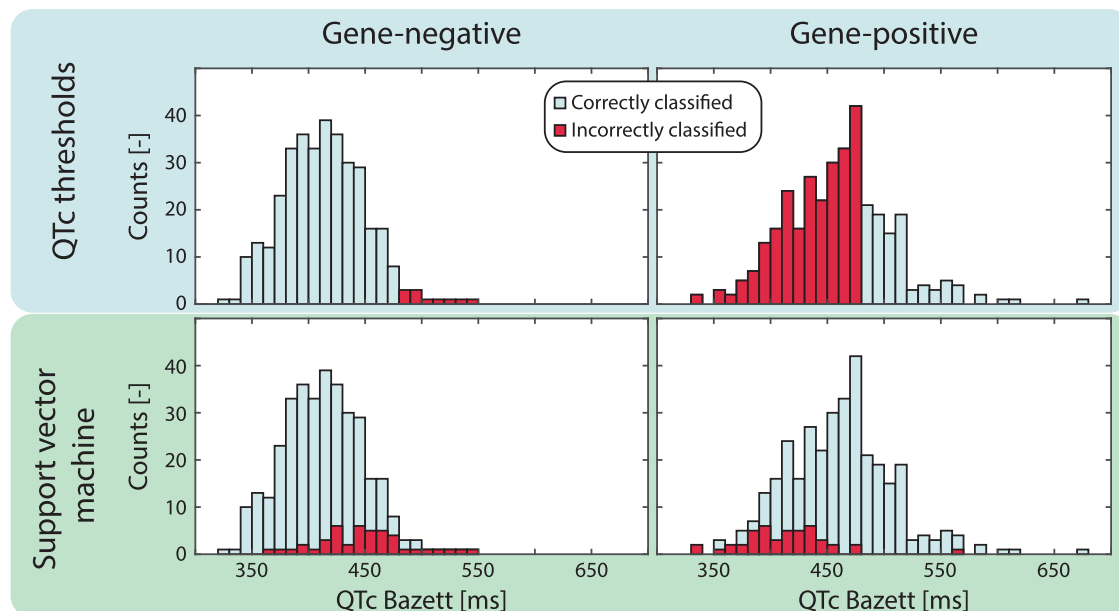
Figure 3 Graphic representation of the added value of the support vector machine with T-wave morphology features on clinically used QTc thresholds. The amount of correctly and incorrectly classified gene-negative subjects (left) and gene-positive subjects (right) based on the QTc-interval cut-off value of 480 ms (top panel) and based on our final support vector machine (bottom panel). The classifications as shown in this figure are the average classifications for each individual patient at YI_{max} obtained from 1000 Monte Carlo cross-validations.

respectively studied 24 h Holter registrations and T-wave morphologies during the brisk-standing-test. Our study only used standard 10-s 12-leads body surface ECGs but could nevertheless show that T-wave morphology markers in these ECGs improve prediction results. Since these standard ECGs are widely available and are part of clinical routine, the added value of being able to improve LQTS diagnosis from these recordings is considerable.

In this study population, gene-negative family members were found to be significantly older than LQTS patients. Not surprisingly, age was a selected feature in both the baseline and the extended model and contributed to the performances of both models. However, since age was a selected feature in both models, the effect of age on the performance of the models is expected to be the same. Therefore, the comparison between both models is still valid.

Next to the support vector machine, a logistic regression model and a bagged random forest were used. From these methods, the support vector machine resulted in the best mean discriminative performance and was therefore used as the machine learning method in this study.

Although it has been shown that Hodges' QTc-intervals are less correlated with heart rate compared with the others,[14] still QTc Bazett is the most commonly used QTc correction method. However, the fact that the only QTc method selected in our baseline model was QTc Hodges might be another argument that the clinical use of QTc Hodges should be re-evaluated.

Limitations

Although the results of this study are promising, there is still room for improvement. First of all, no notch scores are used in our models.

Initially, we implemented the notch score as described by Andersen *et al.*[20] However, we found a very poor agreement between the implemented notch score and visual inspection by two blinded observers. We, therefore, chose to exclude this feature from all models.

Secondly, T_{start} or T_{end} have been manually adjusted for 30 out of 688 ECGs. Although the algorithm seems to work for the majority of ECGs, improving these steps might be necessary before our algorithm can be used on a larger scale.

A third potentially important limitation of the methodology used in this study is that too flat T-waves (<40 μV) have to be excluded even though flat T-waves are a specific aberrant T-wave morphology feature in LQTS patients.

Next, the signal quality of these retrospectively collected ECGs was relatively poor for this study purpose in relatively many cases. Since all ECGs were recorded because of clinical routine, no special care was taken to obtain very high quality ECGs. Though the relatively poor ECG quality might be an explanation for the two limitations described above, future directions should be to increase the robustness of the model to deal with ECGs from daily clinical routine.

Conclusion

In this study, we compared a baseline and an extended model including T-wave morphology inputs, both using support vector machines, to investigate the added value of T-wave morphology markers in diagnosing LQTS. The performances of both models showed that the

model extended with T-wave morphology markers resulted in a better performance in the diagnosis of LQTS. Therefore, it can be concluded that the use of T-wave morphology markers has an added value to distinguish LQTS patients from genotype-negative family members.

Conflict of interest: none declared.

References

1. Wilde AA, Ackerman MJ. Exercise extreme caution when calling rare genetic variants novel arrhythmia syndrome susceptibility mutations. *Heart Rhythm* 2010;**7**:1883–5.
2. Viskin S. The QT interval: too long, too short or just right. *Heart Rhythm* 2009;**6**:711–5.
3. Sy RW, Werf C, Van Der Chattha IS, Chockalingam P, Adler A, Healey JS. Derivation and validation of a simple exercise-based algorithm for prediction of genetic testing in relatives of LQTS probands. *Circulation* 2011;**124**:2187–94.
4. Ackerman MJ, Khositseth A, Tester DJ, Hejlik JB, Shen W-K, Porter CJ. Epinephrine-induced QT interval prolongation: a gene-specific paradoxical response in congenital long QT syndrome. *Mayo Clin Proc* 2002;**77**:413–21.
5. Viskin S, Postema PG, Bhuiyan ZA, Rosso R, Kalman JM, Vohra JK *et al*. The response of the QT interval to the brief tachycardia provoked by standing. *J Am Coll Cardiol* 2010;**55**:1955–61.
6. Postema PG, Neville J, de Jong JS, Romero K, Wilde AA, Woosley RL. Safe drug use in long QT syndrome and Brugada syndrome. *Europace* 2013;**15**:1042–9.
7. Lehmann MH, Suzuki F, Fromm BS, Frankovich D, Elko P, Steinman RT *et al*. T wave 'humps' as a potential electrocardiographic marker of the long QT syndrome. *J Am Coll Cardiol* 1994;**24**:746–54.
8. Moss AJ, Zareba W, Benhorin J, Locati EH, Hall WJ, Robinson JL *et al*. ECG T-wave patterns in genetically distinct forms of the hereditary long QT syndrome. *Circulation* 1995;**92**:2929–34.
9. Chorin E, Havakuk O, Adler A, Steinvil A, Rozovski U, Werf C, van der *et al*. Diagnostic value of T-wave morphology changes during "QT stretching" in patients with long QT syndrome. *Heart Rhythm* 2015;**12**:2263–71.
10. Khositseth A, Hejlik J, Shen WK, Ackerman MJ. Epinephrine-induced T-wave notching in congenital long QT syndrome. *Heart Rhythm* 2005;**2**:141–6.
11. Pan J, Tompkins WJ. A real-time QRS detection algorithm. *IEEE Trans Biomed Eng* 1985;**32**:230–6.
12. Hermans BJM, Vink AS, Bennis FC, Filippini LH, Meijborg VMF, Wilde AAM *et al*. The development and validation of an easy to use automatic QT-interval algorithm. M Baumert, ed. *PLoS One* 2017;**12**:e0184352.
13. Kors JA, Herpen G, van Sittig AC, van Bemmel JH. Reconstruction of the Frank vectorcardiogram from standard electrocardiographic leads: diagnostic comparison of different methods. *Eur Heart J* 1990;**11**:1083–92.
14. Luo S, Michler K, Johnston P, MacFarlane PW. A comparison of commonly used QT correction formulae: the effect of heart rate on the QTc of normal ECGs. *J Electrocardiol* 2004;**37**:81–90.
15. James G, Witten D, Hastie T, Tibshirani R. *An Introduction to Statistical Learning. An Introduction to Statistical Learning: With Applications in R*. New York, NY: Springer New York; 2013.
16. Zou H, Hastie T. selection via the elastic-net. *J R Stat Soc B* 2005;**67**:301–20.
17. Friedman J, Hastie T, Tibshirani R. Regularization paths for generalized linear models via coordinate descent. *J Stat Softw* 2010;**33**:1–22.
18. Priori SG, Wilde AA, Horie M, Cho Y, Behr ER, Berul C *et al*. Executive summary: HRS/EHRA/APHRS expert consensus statement on the diagnosis and management of patients with inherited primary arrhythmia syndromes. *Europace* 2013;**15**:1389–406.
19. Immanuel SA, Sadrieh A, Baumert M, Couderc JP, Zareba W, Hill AP *et al*. T-wave morphology can distinguish healthy controls from LQTS patients. *Physiol Meas* 2016;**37**:1456–73.
20. Andersen MP, Xue JQ, Graff C, Hardahl TB, Toft E, Kanters JK *et al*. A robust method for quantification of IKr-related T-wave morphology abnormalities. *Comput Cardiol* 2007;**34**:341–4.
21. Sugrue A, Noseworthy PA, Kremen V, Bos JM, Qiang B, Rohatgi RK *et al*. Automated T-wave analysis can differentiate acquired QT prolongation from congenital long QT syndrome. *Ann Noninvasive Electrocardiol* 2017;**22**:1–7.
22. Tan AY, Nearing BD, Rosenberg M, Nezafat R, Josephson ME, Verrier RL. Interlead heterogeneity of R- and T-wave morphology in standard 12-lead ECGs predicts sustained ventricular tachycardia/fibrillation and arrhythmic death in patients with cardiomyopathy. *J Cardiovasc Electrophysiol* 2017;**28**:1324–33.
23. Oehler A, Feldman T, Henrikson CA, Tereshchenko LG. QRS-T angle: a review. *Ann Noninvasive Electrocardiol* 2014;**19**:534–42.
24. Min021é A, Ariga R, Neubauer S, Watkins H, Rodr B. Electrocardiographic abnormalities of hypertrophic cardiomyopathy. *Comput Cardiol* 2014;**41**:397–400.